

Comparative study of ZnO and ZnFe<sub>2</sub>O<sub>4</sub> micro and nanoparticle-based screen-printed electrodes in pH sensing

*Original*

Comparative study of ZnO and ZnFe<sub>2</sub>O<sub>4</sub> micro and nanoparticle-based screen-printed electrodes in pH sensing / Madagalam, Mallikarjun; Franceschini, Filippo; Fernandes, Catarina; Rosito, Michele; Padovano, Elisa; Carrara, Sandro; Tagliaferro, Alberto; Bartoli, Mattia; Taurino, Irene. - In: IEEE SENSORS JOURNAL. - ISSN 1530-437X. - ELETTRONICO. - 25:7(2025), pp. 10602-10612. [10.1109/jsen.2025.3543243]

*Availability:*

This version is available at: 11583/3002268 since: 2025-07-31T08:49:25Z

*Publisher:*

IEEE

*Published*

DOI:10.1109/jsen.2025.3543243

*Terms of use:*

This article is made available under terms and conditions as specified in the corresponding bibliographic description in the repository

*Publisher copyright*

IEEE postprint/Author's Accepted Manuscript

©2025 IEEE. Personal use of this material is permitted. Permission from IEEE must be obtained for all other uses, in any current or future media, including reprinting/republishing this material for advertising or promotional purposes, creating new collecting works, for resale or lists, or reuse of any copyrighted component of this work in other works.

(Article begins on next page)

## AUTHOR QUERIES

### AUTHOR PLEASE ANSWER ALL QUERIES

**PLEASE NOTE:** We cannot accept new source files as corrections for your article. If possible, please annotate the PDF proof we have sent you with your corrections and upload it via the Author Gateway. Alternatively, you may send us your corrections in list format. You may also upload revised graphics via the Author Gateway.

Carefully check the page proofs (and coordinate with all authors); additional changes or updates **WILL NOT** be accepted after the article is published online/print in its final form. Please check author names and affiliations, funding, as well as the overall article for any errors prior to sending in your author proof corrections.

AQ:1 = Please note that “Micro and Nanoparticle-based” has been changed as “Microparticle and Nanoparticle-Based” in the article title. Please check and confirm.

AQ:2 = Please confirm or add details for any funding or financial support for the research of this article.

AQ:3 = Please confirm the expansion for the acronym XRD.

AQ:4 = Please confirm whether the edits made in the current affiliation of all the authors are correct.

AQ:5 = Please confirm the city name for Politecnico di Torino.

AQ:6 = Please confirm whether the edits made in the sentence “Mallikarjun Madagalam. . .electrochemical interfaces” are correct.

AQ:7 = Please provide the year of completion when the author Filippo Franceschini received the B.Sc. and M.Sc. degrees.

AQ:8 = Please confirm the retention of the sentence “as an FWO Fellow (Strategic Basic Research).” is correct.

AQ:9 = Please provide the year of completion when the author Sandro Carrara received the Ph.D., master’s, and Diploma degrees.

AQ:10 = The term “Chairman” is considered non-inclusive. Please identify a replacement term from the Inclusive Language Guide found in the IEEE Editorial Style Manual: <https://journals.ieeeauthorcenter.ieee.org/wp-content/uploads/sites/7/IEEE-Editorial-Style-Manual-for-Authors.pdf>

AQ:11 = Please provide a better/higher quality image for the author “Alberto Tagliaferro.”

AQ:12 = Please provide the year of completion when the author Alberto Tagliaferro received the M.Sc. and Ph.D. degrees.

AQ:13 = Please provide the location (city, state code, country) for University of Alberta.

AQ:14 = Please provide the year of completion when the author Irene Taurino received the B.Sc. and dual M.Sc. degrees.

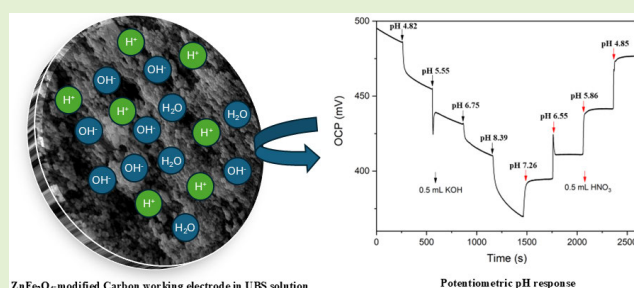
AQ:15 = Please provide the location (city, country) for Aerosol Science and Technology.

# Comparative Study of ZnO and ZnFe<sub>2</sub>O<sub>4</sub> Microparticle and Nanoparticle-Based Screen-Printed Electrodes in pH Sensing

Mallikarjun Madagalam<sup>1</sup>, Student Member, IEEE, Filippo Franceschini, Student Member, IEEE, Catarina Fernandes, Michele Rosito, Elisa Padovano, Sandro Carrara<sup>2</sup>, Fellow, IEEE, Alberto Tagliaferro<sup>3</sup>, Mattia Bartoli<sup>4</sup>, and Irene Taurino, Member, IEEE

**Abstract**—This work presents the application of zinc oxide (ZnO) and zinc ferrite (ZnFe<sub>2</sub>O<sub>4</sub>) for electrochemical pH sensing. ZnO and ZnFe<sub>2</sub>O<sub>4</sub> are synthesized by auto-combustion synthesis method. Field emission scanning electron microscopic (FESEM) images revealed that ZnO particles have pyramid- and spherical-shaped morphology with micrometer dimensions, while ZnFe<sub>2</sub>O<sub>4</sub> particles have spherical shape at the nanoscale. The surface-modified screen-printed electrodes with ZnO and ZnFe<sub>2</sub>O<sub>4</sub> particles are initially characterized by the ferri/ferrocyanide redox couple. Significant improvement in sensitivity (bare carbon:  $6.3 \pm 0.4 \mu\text{A}/\text{mM}$ , ZnO:  $8.5 \pm 0.3 \mu\text{A}/\text{mM}$ , ZnFe<sub>2</sub>O<sub>4</sub>:  $8.9 \pm 0.5 \mu\text{A}/\text{mM}$ ) and rate constant (bare carbon:  $10 \pm 1 \text{ms}^{-1}$ , ZnO:  $46 \pm 4 \text{ms}^{-1}$ , ZnFe<sub>2</sub>O<sub>4</sub>:  $42 \pm 3 \text{ms}^{-1}$ ) is observed with the surface-modified sensors. Chronopotentiometric pH response of the sensors showed hysteresis behavior with pH loop. No interference effects are observed, and the pH sensitivity of the bare carbon sensor ( $23.9 \pm 1.4 \text{mV}/\text{pH}$ ) is increased by the introduction of ZnO ( $38.1 \pm 1.3 \text{mV}/\text{pH}$ ) and ZnFe<sub>2</sub>O<sub>4</sub> ( $37.2 \pm 1.1 \text{mV}/\text{pH}$ ) particles. Stability of the pH response is discussed, and ways for its improvement are proposed.

**Index Terms**—Microparticles, nanoparticles, potentiometric pH sensor, sensor stability, zinc ferrite (ZnFe<sub>2</sub>O<sub>4</sub>), zinc oxide (ZnO).



## I. INTRODUCTION

ELECTROCHEMICAL pH sensing is valued for its high sensitivity, rapid response, and adaptability to a wide range of environments, making it a versatile solution in fields such as clinical diagnostics [1], environmental monitoring [2], water quality assessment [3], [4], and industrial process control [5]. These sensors operate based on the electrochemical interaction between a pH-sensitive material and hydrogen ions (H<sup>+</sup>) in a solution, allowing for real-time, in situ measurements of acidity, neutrality, or alkalinity of a solution [6].

Electrochemical pH sensors typically work through potentiometric, amperometric, or conductometric approaches. The most common type is the potentiometric pH sensor, which measures the potential difference between a pH-sensitive

working electrode (WE) (such as glass electrodes or metal oxides) and a reference electrode (RE) (typically Ag/AgCl) immersed in the solution. The potential generated at the WE is proportional to the activity of H<sup>+</sup> ions, which are related to the solution's pH value through Nernst equation [6], [7], [8].

Metal oxide nanomaterials have emerged as highly effective materials for electrochemical pH sensing due to their excellent electrochemical properties, stability, and sensitivity to hydrogen ions (H<sup>+</sup>) in solutions. Their unique structural, electrical, and chemical characteristics make them suitable for a wide range of pH sensing applications [1], [6], [9], [10]. In environmental applications, titanium dioxide (TiO<sub>2</sub>) [11] and zinc oxide (ZnO) [3], [12] nanomaterials have been employed in pH sensors to monitor water quality due to their wide bandgap [13], [14]. These sensors can detect shifts in pH caused by contaminants in rivers, lakes, or oceans, providing crucial data for water management. Nickel oxide (NiO) [15] and copper oxide (CuO) [6], [9], [16] nanoparticles are also commonly used in soil pH sensors due to their robust sensing capabilities in harsh environments.

In clinical diagnostics, monitoring pH is vital for tracking physiological parameters such as blood acidity (pH of blood)

Received 3 January 2025; accepted 4 February 2025. The associate editor coordinating the review of this article and approving it for publication was Dr. Xiaoshan Zhu. (Corresponding author: Mallikarjun Madagalam.)

Please see the Acknowledgment section of this article for the author affiliations.

This article has supplementary downloadable material available at <https://doi.org/10.1109/JSEN.2025.3543243>, provided by the authors.

Digital Object Identifier 10.1109/JSEN.2025.3543243

or the pH of interstitial fluids, which are critical in conditions like acidosis or alkalosis [1]. Iridium oxide ( $\text{IrO}_x$ ) [8], [17] and ruthenium oxide ( $\text{RuO}_2$ ) [1], [6], [10], [18], [19] are used to develop pH sensors with super Nernstian behavior that can be integrated into biomedical devices, including wearable and implantable sensors. These materials exhibit fast response times and stability under physiological conditions. Tin oxide ( $\text{SnO}_2$ ) [6], [18], [20] nanomaterials are also explored for implantable pH sensors due to their nontoxic nature and high sensitivity to pH changes, which are essential features for detecting pH changes in tissue environments during medical treatments. Tungsten oxide ( $\text{WO}_3$ ) is also used to develop pH sensors for clinical diagnostics [21], [22].

Spinel oxides are another class of multitransition metal oxides such as zinc ferrite ( $\text{ZnFe}_2\text{O}_4$ ) and nickel ferrite ( $\text{NiFe}_2\text{O}_4$ ). The spinels possess a crystal structure of the form  $\text{AB}_2\text{O}_4$  (A—metal cation with “+2” oxidation state and B—metal cation with “+3” oxidation state) with excellent chemical stability and electrical neutrality [23]. Several spinel oxide nanomaterials are used as sensing materials in electrochemical sensing applications for drug detection [24]. An improvement of the electrochemical sensing response is possible due to the tunability of their crystal structure. Their composition can be easily modified maintaining the chemical stability of the structure [25], [26], [27], [28], [29]. The spinel can be normal, inverse, or mixed with different cations occupying different sites in the crystal structure and leading to different electrochemical performance due to the change in their semiconducting nature either from  $p$  to  $n$  or from  $n$ - to  $p$ -type [25], [26]. The magnetic nature (ferromagnetic and antiferromagnetic behavior leading to electron scattering effects and charge trapping) of the spinel materials also plays an important role in the conductivity of spinel oxides [30] which in turn can affect the electrochemical sensing performance. This class of spinel nanomaterials is not explored as pH sensing electrode materials in the literature as far as our knowledge is concerned. Therefore, in this work, we investigate the capability of  $\text{ZnFe}_2\text{O}_4$  normal spinel material to act as an electrode sensing material of pH.

$\text{ZnO}$  and  $\text{ZnFe}_2\text{O}_4$  particles are synthesized and characterized using different techniques. Commercial screen-printed electrodes (SPEs) are used as an electrochemical sensing cell and the surface of the WE is modified with the newly synthesized materials. The electrochemical behavior of the new sensors is first assessed using the well-known ferri/ferrocyanide probe molecule, then their performance as pH sensors is assessed. Different performance characteristics of pH sensors such as hysteresis, sensor stability, sensitivity, and interference effects are presented and discussed.

## II. MATERIALS AND METHODS

### A. Chemicals

Zinc nitrate ( $\text{Zn}(\text{NO}_3)_2 \cdot 6\text{H}_2\text{O}$ ), iron nitrate ( $\text{Fe}(\text{NO}_3)_3 \cdot 9\text{H}_2\text{O}$ ),  $\text{C}(\text{NH}_2)_2\text{O}$  (Urea), Butanol ( $\text{C}_4\text{H}_{10}\text{O}$ ), potassium hexacyanoferrate(II) ( $\text{K}_4\text{Fe}(\text{CN})_6$ ), potassium hexacyanoferrate(III) ( $\text{K}_3\text{Fe}(\text{CN})_6$ ), acetic acid ( $\text{CH}_3\text{COOH}$ ), potassium nitrate ( $\text{KNO}_3$ ), boric acid ( $\text{H}_3\text{BO}_3$ ), phosphoric acid ( $\text{H}_3\text{PO}_4$ ), potassium hydroxide (KOH), and nitric acid

( $\text{HNO}_3$ ) are purchased from Sigma Aldrich and used without any further purification.

### B. Material Synthesis

A simple and cost-effective auto-combustion synthesis is used to synthesize nanomaterials based on our previous work [25]. Synthesis of  $\text{ZnFe}_2\text{O}_4$  nanoparticles is reported in our previous work [25], [31].  $\text{ZnO}$  is synthesized by using only  $\text{Zn}(\text{NO}_3)_2 \cdot 6\text{H}_2\text{O}$  following the same process as  $\text{ZnFe}_2\text{O}_4$  synthesis.

### C. Preparation of Universal Buffer Solution (UBS)

UBS covering the pH range from 2 to 12 is prepared to characterize electrochemical sensors. A measure of 0.3 mL (0.01 M) of  $\text{CH}_3\text{COOH}$ , 5.05 g (0.1 M) of  $\text{KNO}_3$ , 0.31 g (0.01 M) of  $\text{H}_3\text{BO}_3$ , and 0.58 mL (0.01 M) of  $\text{H}_3\text{PO}_4$  are mixed with 0.5 L of deionized (DI) water in a glass container. The mixture is kept in an ultrasonic bath for 5 min to dissolve all the chemicals and obtain a final homogeneous solution.

### D. Apparatus

Field emission scanning electron microscopic (FESEM) images are collected utilizing a Zeis SupraTM 50 (Oberkochen, Germany) to examine the nanomaterial's morphology. The crystal structure of the materials is determined by X-ray powder diffraction (XRD) using a Panalytical Empyrean diffractometer (Malvern Panalytical, Malvern, U.K.). The XRD analysis of the powder samples is performed at room temperature using a Bragg–Brentano setup with  $\text{Cu K}\alpha$  ( $\lambda = 1.5418 \text{ \AA}$ ) radiation at 40 kV and a current of 40 mA. The analysis is carried out using a time step of 60 s and a step size of  $0.013^\circ/\text{s}$ , covering a  $2\theta$  range from  $10^\circ$  to  $70^\circ$ . Palmsens potentiostat with PStTrace 5.9 is used to perform cyclic voltammetry (CV) in solutions containing ferri/ferrocyanide. Metrohm Autolab with Nova 2.1 is used for electrochemical impedance spectroscopic (EIS) studies and chronopotentiometric pH sensing.

### E. Electrochemical Sensors

Commercial screen-printed carbon WE (area  $0.12 \text{ cm}^2$ ) and carbon counter electrode (CE) on a ceramic substrate along with an external double junction  $\text{Ag}/\text{AgCl}$  RE are used as electrodes for ferri/ferrocyanide sensing. The same method as reported in the literature [25] is adopted to prepare the nanomaterial solutions and the surface of the carbon WE is modified using the drop-casting technique as reported previously [25], [31], [32].

### F. Electrochemical Measurements

CV is used to characterize the sensors performance for the detection of ferri/ferrocyanide redox couple with a potential window ranging from  $-0.4$  to  $0.8 \text{ V}$  at a scan rate of  $100 \text{ mV/s}$  in phosphate buffer (PB) at pH 7. Scan rate analysis is performed by changing the scan rate from  $25 \text{ mV/s}$  to  $125 \text{ mV/s}$  in steps of  $25 \text{ mV/s}$ . Calibration of the sensors is conducted by recording cyclic voltammograms in the concentration range

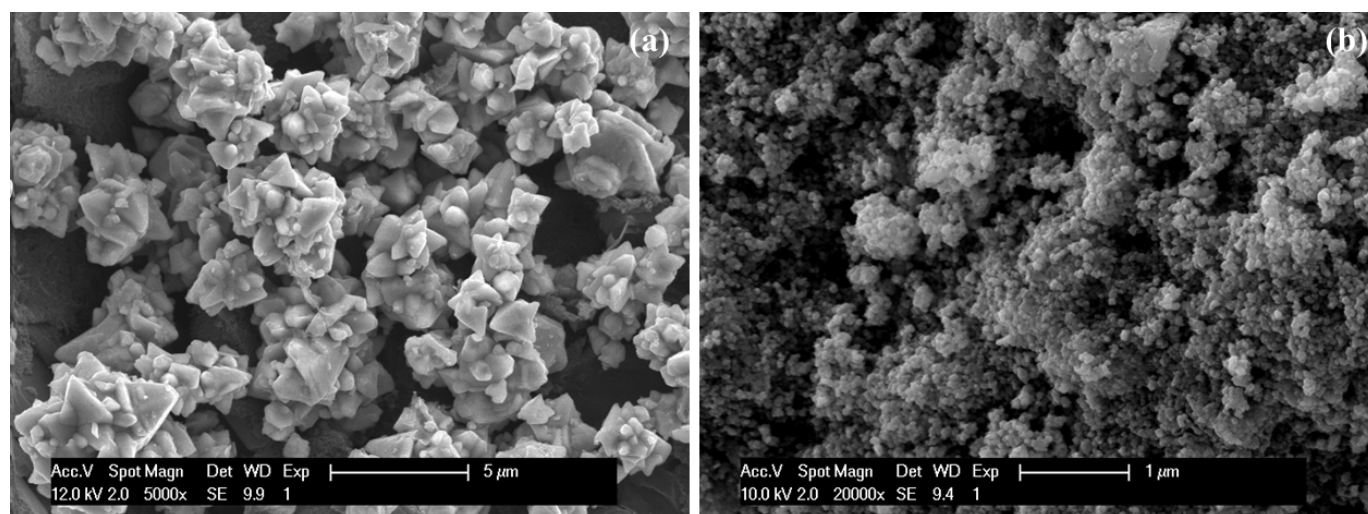


Fig. 1. FESEM images of (a) ZnO with 5k $\times$  and (b) ZnFe<sub>2</sub>O<sub>4</sub> with 20k $\times$  magnification, respectively.

164 from 1 to 8 mM of ferri/ferrocyanide redox couple. EIS  
 165 is performed in the frequency from 0.1 to 100 kHz with  
 166 10 points/decade at an amplitude of 5 mV. Chronopotentiometric  
 167 experiments are conducted for pH initially in the full  
 168 loop of 2-12-2 and in the physiologically relevant pH range  
 169 of 5-8.5. The RE and CE probes of the Autolab are coupled  
 170 together, and the solution is continuously stirred at 500 r/min.  
 171 Open-circuit potential (OCP) is recorded with time and the  
 172 average of the last 60 s of the response of OCP before any  
 173 pH change in solution is plotted against the pH value for the  
 174 calibration. The slope of the plot is reported as the sensitivity  
 175 of the sensors. Interference measurements are conducted using  
 176 30 mM KCl and 5 mM NaCl to verify the robustness of the  
 177 sensor toward interfering ions.

### 178 III. RESULTS AND DISCUSSION

#### 179 A. Material Characterization

180 Fig. 1 shows the FESEM images of ZnO and ZnFe<sub>2</sub>O<sub>4</sub>  
 181 particles-modified carbon surface. ZnO particles have a pyramidal  
 182 shape at microscale, while some smaller particles exhibit  
 183 a different morphology like spherical one. ZnFe<sub>2</sub>O<sub>4</sub> particles  
 184 show spherical-shaped morphology. A certain amount of  
 185 aggregation is observed in both materials that are possibly  
 186 due to the adopted synthesis method [25], [33] as it provides  
 187 a weak control over the particle growth kinetics.

188 The XRD patterns of ZnFe<sub>2</sub>O<sub>4</sub> and ZnO are shown in  
 189 Fig. 2. For ZnFe<sub>2</sub>O<sub>4</sub>, the experimental pattern fully matches  
 190 with the normal spinel Franklinite (ZnFe<sub>2</sub>O<sub>4</sub>, reference code  
 191 01-089-4926). Some low-intensity peaks are noticed in the  
 192  $2\theta$  range between 30° and 37°: these peaks are compatible  
 193 with the most intense peaks of ZnO (reference code 01-080-0075)  
 194 and iron oxide (Fe<sub>2</sub>O<sub>3</sub>, reference code 01-085-0987) in accordance  
 195 with previous studies [25], [26]. For ZnO, the XRD pattern  
 196 neatly matches with the ZnO one (reference code 01-080-0075).  
 197 The low-intensity peak at low angles is attributed to graphite,  
 198 which might be present as an impurity due to the graphite reactor  
 199 used for the material synthesis. Crystallite size of the materials  
 200 is calculated using Scherrer's method [25], [26]. ZnFe<sub>2</sub>O<sub>4</sub> has  
 201 an average crystallite size of 35.2  $\pm$  3.3 nm, while ZnO has an  
 202 average

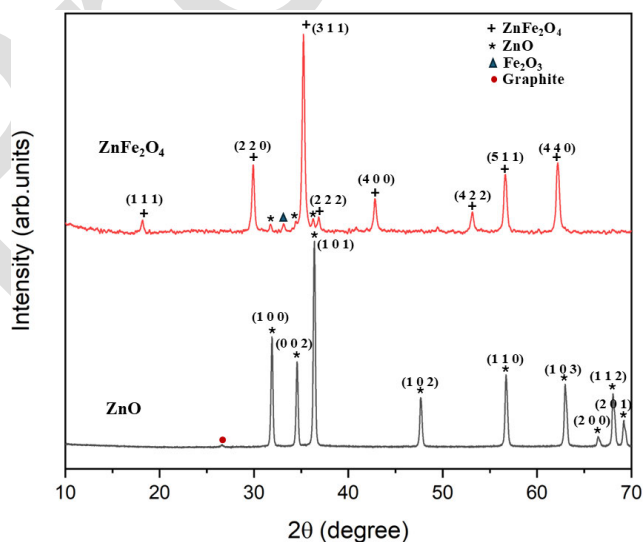


Fig. 2. XRD patterns of ZnFe<sub>2</sub>O<sub>4</sub> and ZnO particles synthesized by auto-combustion.

203 crystallite size of 45.7  $\pm$  1.3 nm. In the case of ZnO-particles,  
 204 particles are formed by abnormal asymmetric growth leading  
 205 to the micrometer dimensions of particles, as evidenced in  
 206 Fig. 1.

#### 207 B. Electrochemical Characterization

208 Fig. 3 shows the cyclic voltammograms of the bare,  
 209 ZnFe<sub>2</sub>O<sub>4</sub>, and ZnO sensors characterized in 4 mM  
 210 ferri/ferrocyanide redox couple in 0.1 M PB at pH 7 at  
 211 a scan rate of 100 mV/s. The introduction of nanostructured/  
 212 microstructured materials has enhanced the performance  
 213 of screen-printed carbon electrodes. The oxidation peak current  
 214 ( $I_{pa}$ ) is increased [ $\sim$ 14  $\mu$ A:  $I_{pa}$  = 44.1  $\pm$  0.6  $\mu$ A  
 215 (ZnFe<sub>2</sub>O<sub>4</sub>), 44.3  $\pm$  0.4  $\mu$ A (ZnO)] and the anodic peak potential  
 216 (oxidation peak potential:  $E_{pa}$ ) is decreased [ $\sim$ 70 mV:  
 217  $E_{pa}$  = 413  $\pm$  3 (ZnFe<sub>2</sub>O<sub>4</sub>), 407  $\pm$  3 mV (ZnO)] compared to  
 218 bare carbon sensor ( $I_{pa}$  = 30.6  $\pm$  1.4  $\mu$ A,  $E_{pa}$  = 483  $\pm$  7 mV).

219 Cyclic voltammograms obtained at various scan rates are  
 220 depicted in Fig. S1 for bare carbon, ZnFe<sub>2</sub>O<sub>4</sub>, and ZnO  
 221 sensors. The anodic ( $I_{pa}$ ) and cathodic peak currents ( $I_{pc}$ )

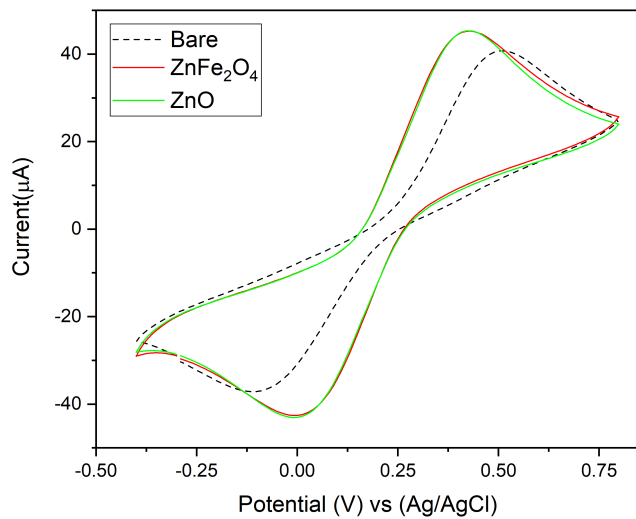


Fig. 3. Cyclic voltammograms of different sensors at a scan rate of 100 mV/s. (Electrolytic solution: 4 mM ferri/ferrocyanide in PB (0.1 M) at pH 7).

TABLE I

ELECTROACTIVE SURFACE AREA AND INTERFACE IMPEDANCES IN CHARACTERIZING FERRI/FERROCYANIDE REDOX COUPLE ON BARE CARBON AND SURFACE-MODIFIED SENSORS

Sensor	$A_{RS}$ (cm <sup>2</sup> )	$R_s$ (Ω)	$R_p$ (kΩ)
Bare	$0.27 \pm 0.05$	166	17.2
ZnFe <sub>2</sub> O <sub>4</sub>	$0.49 \pm 0.03$	146	13.4
ZnO	$0.49 \pm 0.02$	139	11.8

increased with the increase in scan rate and varied linearly with the square root of the scan rate ( $\sqrt{\nu}$ ) in the range 25–125 mV/s, as shown in Fig. S2. The peak currents linear regression equations with their regression coefficients, confirming the high level of linearity, are listed in Table S1. Absolute redox current peak values are plotted in Fig. S3 to show the differences between the oxidation and reduction peak currents. The redox peak current ratios with scan rate are reported in Table S2, and the ratio  $I_{pa}/I_{pc}$  is  $\approx 1$ . Electroactive surface area ( $A_{RS}$ ) of the sensors is calculated using Randles–Sevcik equation [26] and reported in Table I. It is observed that the electroactive surface area of the sensors is increased due to the presence of nanoparticle/microparticle of ZnFe<sub>2</sub>O<sub>4</sub>/ZnO on the carbon surface compared to the bare carbon sensor. Both ZnFe<sub>2</sub>O<sub>4</sub> and ZnO-based sensors have a similar electroactive surface area indicating the same loading of the nanoparticle/microparticle on the carbon surface that participates in the electrochemical reaction with ferri/ferrocyanide redox couple.

The peak-to-peak separation ( $\Delta E_p = E_{pa} - E_{pc}$ , where  $E_{pc}$  is the cathodic peak potential or reduction peak potential) lowered by 150 mV compared to bare carbon sensor due to the presence of either ZnO or ZnFe<sub>2</sub>O<sub>4</sub> particles. The ZnO-based sensor showed the lowest  $\Delta E_p$  of  $387 \pm 9$  mV, while the ZnFe<sub>2</sub>O<sub>4</sub> sensor and bare carbon sensor exhibited a  $\Delta E_p$  of  $397 \pm 7$  and  $547 \pm 9$  mV, respectively. As the electron transfer kinetics are directly related to  $\Delta E_p$ , the

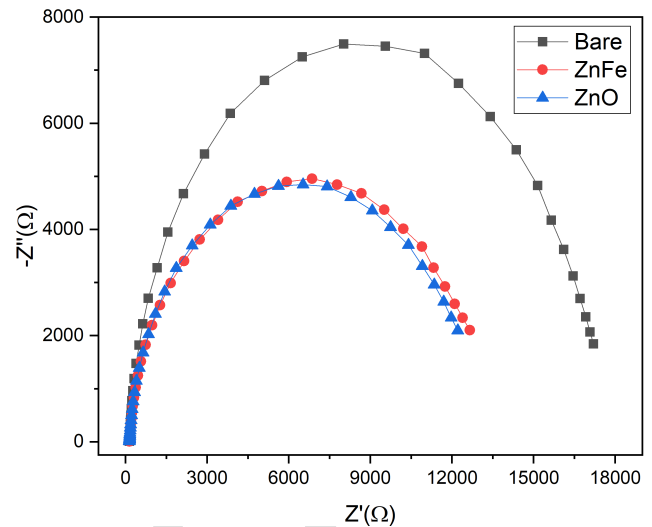


Fig. 4. Nyquist plots of different sensors in 4 mM ferri/ferrocyanide in PB (0.1 M) at pH 7. Frequency range is 0.5–100 kHz with 10 points per decade at an amplitude of 5 mV.

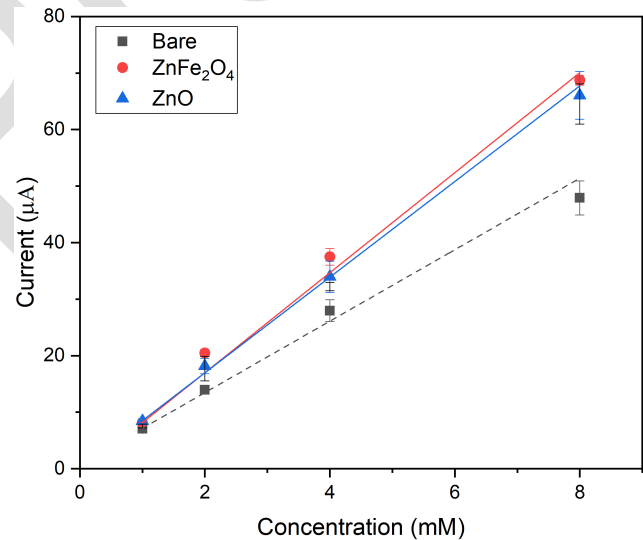


Fig. 5. Calibration of sensors for concentrations of ferri/ferrocyanide redox couple in PB (0.1 M) up to 8 mM.

lower  $\Delta E_p$  indicates faster electrochemical reactions with high reversibility. In Figs. S4 and S5, the redox peak positions  $E_{pa}$  and  $E_{pc}$ , and  $\Delta E_p$  are plotted and a linear variation against  $\ln(\nu)$  is observed. The linear regression equations with their coefficients are reported in Tables S3 and S4, respectively. Half-potential ( $E_{1/2} = (E_{pa} + E_{pc})/2$ ) is shown in Fig. S6 and has almost a constant relation with  $\ln(\nu)$  is observed. The redox peak current ratio,  $\Delta E_p$ , and  $E_{1/2}$  suggest that the interface is a quasi-reversible electrochemical interface from Randles–Sevcik theory [34], [35]. Following the equations from the Laviron model [25], [36], [37], the electron transfer rate coefficient “ $\alpha$ ” and kinetic rate constant “ $k_s$ ” using  $\Delta E_p$  ( $\nu = 100$  mV/s) and  $n = 1$ , are calculated and presented in Table II.

EIS is performed to study the impedance properties of the electrochemical interface between 4 mM ferri/ferrocyanide redox couple and different sensors. Nyquist plots of bare, ZnFe<sub>2</sub>O<sub>4</sub>, and ZnO-based sensors are reported in Fig. 4. The Nyquist profiles of the sensors show only semicircles

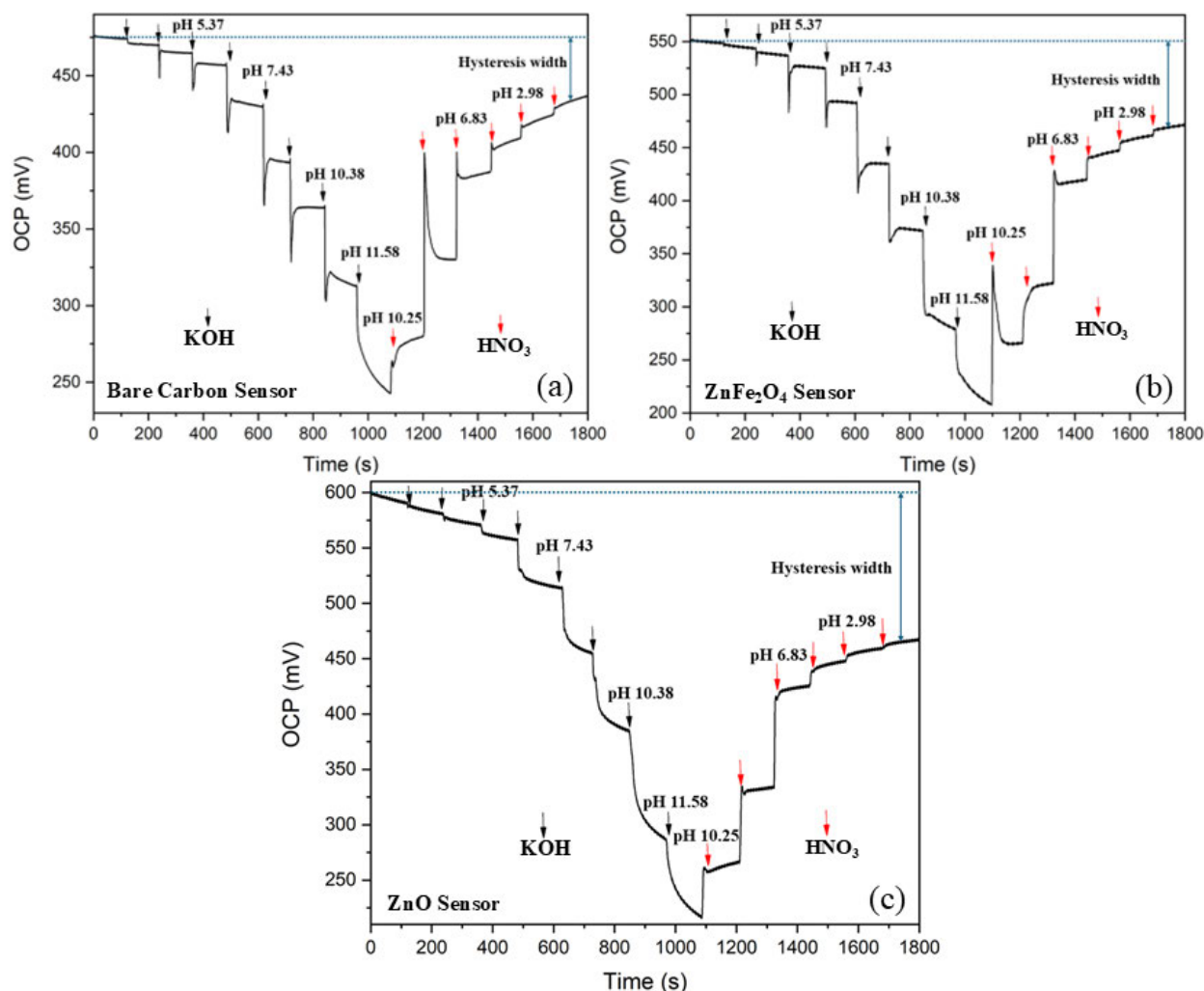


Fig. 6. Chronopotentiometric response of (a) bare, (b) ZnFe<sub>2</sub>O<sub>4</sub>, and (c) ZnO pH sensors showing the hysteresis effect in pH loop 2-12-2.

TABLE II  
ELECTROCHEMICAL PARAMETERS IN CHARACTERIZING  
FERRI/FERROCYANIDE REDOX COUPLE ON BARE  
CARBON AND SURFACE-MODIFIED SENSORS

Sensor	$\alpha$	$\Delta E_p$ (mV)	$k$ (ms <sup>-1</sup> )
Bare	0.47 ± 0.01	547 ± 9	9.97 ± 0.78
ZnFe <sub>2</sub> O <sub>4</sub>	0.49 ± 0.01	397 ± 7	41.8 ± 2.6
ZnO	0.496 ± 0.002	387 ± 9	46 ± 4

268 associated with charge transfer kinetic limitations. Therefore,  
269 Randles equivalent circuit model with a series resistance  
270 ( $R_s$ ), charge transfer resistance ( $R_p$ ), and a constant phase  
271 element (CPE) are used to fit the obtained Nyquist plots  
272 of bare, ZnFe<sub>2</sub>O<sub>4</sub>, and ZnO-modified sensors without any  
273 Warburg impedance (diffusion-controlled) as shown in Fig. S7.  
274 From the circuit fitting, series (solution) resistance ( $R_s$ ) and  
275 charge transfer resistance ( $R_p$ ) of the sensors are extracted  
276 and reported in Table I. The charge transfer resistance of the  
277 ZnFe<sub>2</sub>O<sub>4</sub> and ZnO-based sensors is significantly lower than  
278 the bare carbon sensor supporting the higher electron transfer  
279 rate constant. ZnO-based sensor showed 1.6 k $\Omega$  lower charge

280 transfer resistance with similar CPE parameters compared to  
281 ZnFe<sub>2</sub>O<sub>4</sub>-based sensor supporting its higher electron transfer  
282 rate (higher “ $k$ ”).

283 The sensors are calibrated by taking the average response  
284 of three sensors of each type, and the calibration plots are  
285 shown in Fig. 5. Sensitivity is computed with reference to the  
286 oxidation peaks of the ferri/ferrocyanide redox couple in the  
287 concentration range 1–8 mM. The bare carbon sensor has a  
288 sensitivity of 6.3 ± 0.4  $\mu$ A/mM, while the ZnFe<sub>2</sub>O<sub>4</sub>-based  
289 sensor and the ZnO-based sensor have sensitivities of 8.9 ±  
290 0.5 and 8.5 ± 0.3  $\mu$ A/mM, respectively. Though there are  
291 significant differences in crystallite size and morphology, the  
292 materials have shown similar electrochemical performance ( $k$   
293 and sensitivity) which might be due to their similar electroac-  
294 tive surface area and charge transfer resistance.

295 Fig. 6 shows the chronopotentiometric response of bare  
296 carbon, ZnFe<sub>2</sub>O<sub>4</sub>, and ZnO-based sensors in the full pH  
297 loop of 2-12-2 (with 15 different pH values reported in the  
298 supporting information Table S5). The response at each pH is  
299 measured for two minutes (total time span of 30 min), and  
300 it is observed that ZnO has the higher initial OCP (lowest  
301 pH values). Moreover, there is huge shift in OCP after pH  
302 10 for all sensors. In the reverse pH from basic to acidic  
303 region, the OCP is similar in the surface-modified sensors

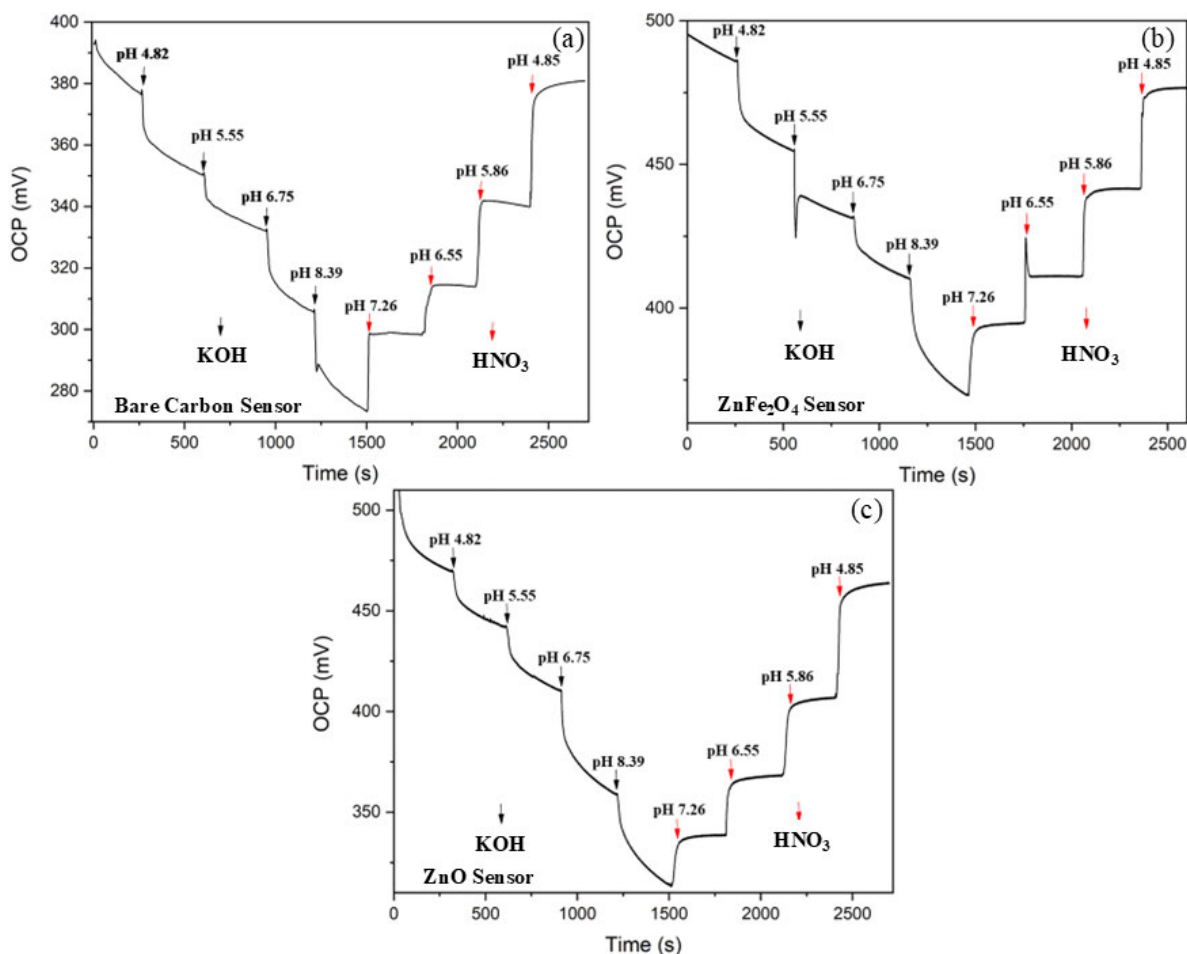


Fig. 7. Chronopotentiometric response of (a) bare, (b)  $\text{ZnFe}_2\text{O}_4$ , and (c)  $\text{ZnO}$  pH sensors with reduced hysteresis effect in pH loop 4.5–8.5–4.5.

304 compared to the initial OCP from acidic to basic region.  
 305 These differences in response leads to a phenomenon called  
 306 “hysteresis” in pH sensors especially in the case of metal  
 307 oxide-based pH sensors [6]. The potential difference from  
 308 initial response to the final response in the complete pH loop  
 309 is called the “hysteresis width” as indicated in Fig. 6. The  
 310  $\text{ZnO}$ -based sensor has the highest hysteresis width of 133 mV,  
 311 bare carbon sensor has the lowest width of 39 mV, and the  
 312  $\text{ZnFe}_2\text{O}_4$ -based sensor has a hysteresis width of 81 mV. The  
 313 hysteresis width defines the functionality of a pH sensor and  
 314 the pH range in which the sensor can be utilized. The lower  
 315 the hysteresis width, the better the performance of the sensor  
 316 in that pH range. As reported before, the hysteresis behavior  
 317 depends on the pH looping (pH range in which the sensor is  
 318 operated) [38]. Since our main interest is in the physiological  
 319 pH range, the sensors are characterized in the pH loop  
 320 4.5–8.5–4.5 (with nine different pH values with a total time  
 321 span of 45 min) as shown in Fig. 7. It is clearly observed that  
 322 the hysteresis behavior is reduced to 3, 18, and 44 mV for  
 323 bare carbon,  $\text{ZnFe}_2\text{O}_4$ , and  $\text{ZnO}$ -based sensors, respectively.  
 324 This is significantly lower compared to the previous pH loop  
 325 proving that the hysteresis behavior is pH loop-dependent.

326 Stability of the pH sensors is another important performance  
 327 factor. As is clear from Figs. 6 and 7, the potentiometric  
 328 response is not reaching a steady-state value when the pH is  
 329 changing from lower to higher values by the addition of KOH

330 solution. To understand the sensors’ stability, the response  
 331 is recorded at different pH values for longer times (10 and  
 332 20 min after each change in pH value) as presented in Fig. 8.  
 333 A drift over time is still observed without reaching any steady-  
 334 state value. The response starts to stabilize immediately after  
 335 the addition of  $\text{HNO}_3$  solution into the solution under test.  
 336 To understand this effect, it is important to consider how  
 337 a pH sensor works. When the sensor is immersed into the  
 338 test solution, the hydroxide ( $\text{OH}^-$ ) ions get attracted by the  
 339 electrode surface due to the dissociative adsorption of water.  
 340 This adsorption leads to a potential difference between the  
 341 WE and the RE. Due to the addition of more KOH solution  
 342 into the test UBS solution, the sensor’s surface is enriched  
 343 with more  $\text{OH}^-$  ions, leading to a difference in the potential  
 344 between WE and RE. When the  $\text{HNO}_3$  solution is added,  
 345 the response starts to stabilize immediately as we introduce  
 346  $\text{H}^+$  ions. This is due to the faster diffusion of  $\text{H}^+$  ions (and  
 347 so faster protonation of the electrode surface) compared to  
 348 the process of interaction of  $\text{OH}^-$  ions with the electrode  
 349 surface [6]. To improve the stability of the sensors, instead  
 350 of using KOH as the base stock solution, bicarbonates such as  
 351  $\text{KHCO}_3$  or  $\text{NaHCO}_3$  can be employed. This might improve the  
 352 stability of the potential response as well as the pH sensitivity  
 353 of the sensors. When the pH of the solution under investigation  
 354 is controlled with KOH and  $\text{HNO}_3$ , the sensors are calibrated  
 355 in the pH range mentioned above to compare the OCP. When

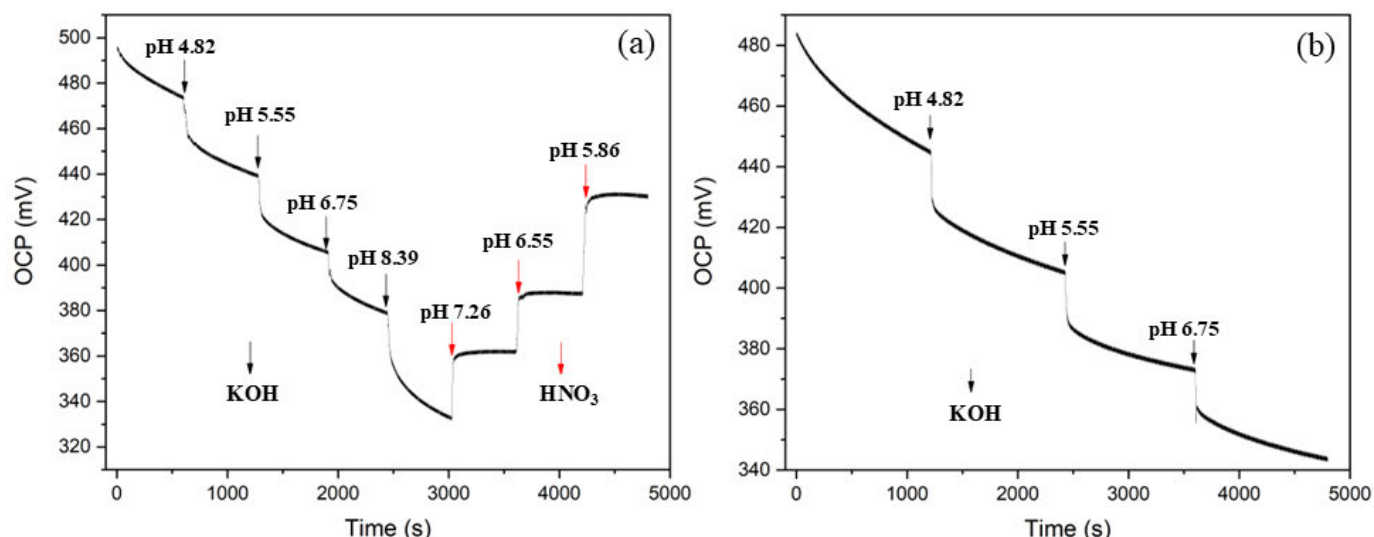


Fig. 8. Stability tests: chronopotentiometric response of ZnFe<sub>2</sub>O<sub>4</sub> pH sensor with longer stabilization times [(a) 10 and (b) 20 minutes of waiting time in between subsequent pH changes] after each pH change in the range between 4.5 and 8.5.

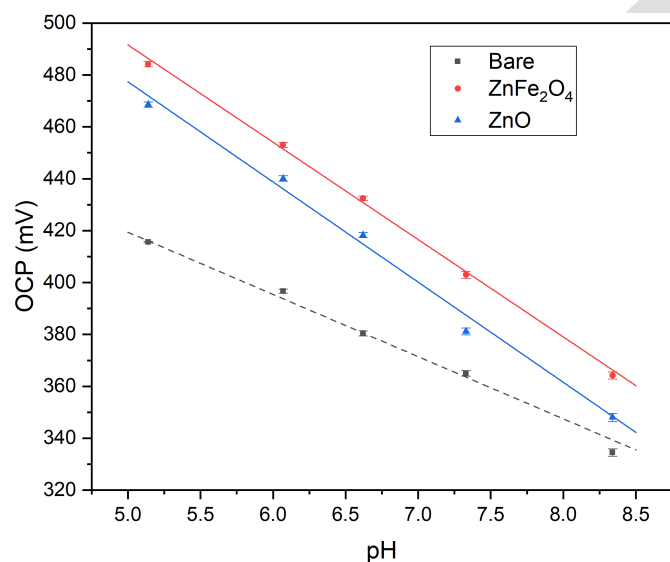


Fig. 9. Calibration of bare carbon, ZnFe<sub>2</sub>O<sub>4</sub>, and ZnO pH sensors in the pH between 5 and 8.5.

HNO<sub>3</sub> is used after KOH in continuous measurements, the sensitivity of the sensors is higher, according to the calibration plots shown in Fig. S8. However, this is unreliable because the OCP response is unstable in the first case when KOH is used, which affects the OCP levels in the second case when HNO<sub>3</sub> is used for pH control. The response time of the sensors is difficult to investigate due to unstable response in the case of KOH; therefore, the response time is reported for the second case when HNO<sub>3</sub> is used for pH control. The bare, ZnFe<sub>2</sub>O<sub>4</sub>, and ZnO-based sensors showed response times ( $T_{95}$ ) of 5, 80, and 95 s, respectively. These times are just indicative but not reliable due to unstable continuous OCP measurements with KOH for pH control.

To assess the performance of the electrodes as pH sensors, three freshly prepared electrodes of each type are taken, and the potential response is measured for three minutes as reported in Fig. S9. The average potential response in the last

60 s before changing the pH is considered to calibrate the sensors in the pH range between 5 and 8.5. pH calibration of the sensors is presented in Fig. 9. Bare carbon sensor, ZnFe<sub>2</sub>O<sub>4</sub>, and ZnO-based sensors have shown sensitivities of  $23.9 \pm 1.4$ ,  $37.3 \pm 1.1$ , and  $38.1 \pm 1.3$  mV/pH, respectively. The presence of either ZnFe<sub>2</sub>O<sub>4</sub> or ZnO significantly improved the pH sensing performance of bare carbon sensor, resulting in an increase of sensitivity of around 60%. pH sensing response is usually analyzed with the Nernst equation [6] as written below

$$E = E_0 - \frac{2.303RT}{nF} \text{pH} \quad (1)$$

where  $E$  is the Nernst potential,  $E_0$  is the standard surface potential,  $R$  is the universal gas constant,  $T$  is the temperature, and “ $n$ ” is the number of electrons transferred in the reaction. At atmospheric conditions with  $T = 25^\circ\text{C}$  for one electron process (i.e.,  $n = 1$ ), the slope of the plot ( $E$  versus pH) is 59 mV/pH. This response is usually termed as Nernstian response for pH. Though for our sensors the response is not Nernstian, we observed a significant increase with respect to bare sensor, proving the potential of ZnFe<sub>2</sub>O<sub>4</sub> or ZnO in pH sensing applications.

The ZnO particles have a pyramid shape where the sides and long edges of the particles are electroactive, whereas ZnFe<sub>2</sub>O<sub>4</sub> has (close to) uniform spherical-shaped particles. Another difference is in the crystal structure which is hexagonal for ZnO microparticles, while ZnFe<sub>2</sub>O<sub>4</sub> particles exhibit a complex normal spinel where the metal centers of Fe and Zn play an important role in the electrochemical activity of the sensors [24], [39]. ZnO is a wide bandgap material (either p- or n-type semiconductor) with a bandgap around 3.2 eV [40], whereas ZnFe<sub>2</sub>O<sub>4</sub> (n-type semiconductor) has a smaller bandgap of about 2.5 eV [25], [26]. Even though they have these differences, we have observed that a comparable electroactive surface area (from ferri/ferrocyanide sensing), charge transfer resistance [kinetic limited reactions without diffusion limitations from Nyquist plots (see Fig. 4)], electron transfer rate constant (“ $k$ ”) and sensitivity in pH sensing for

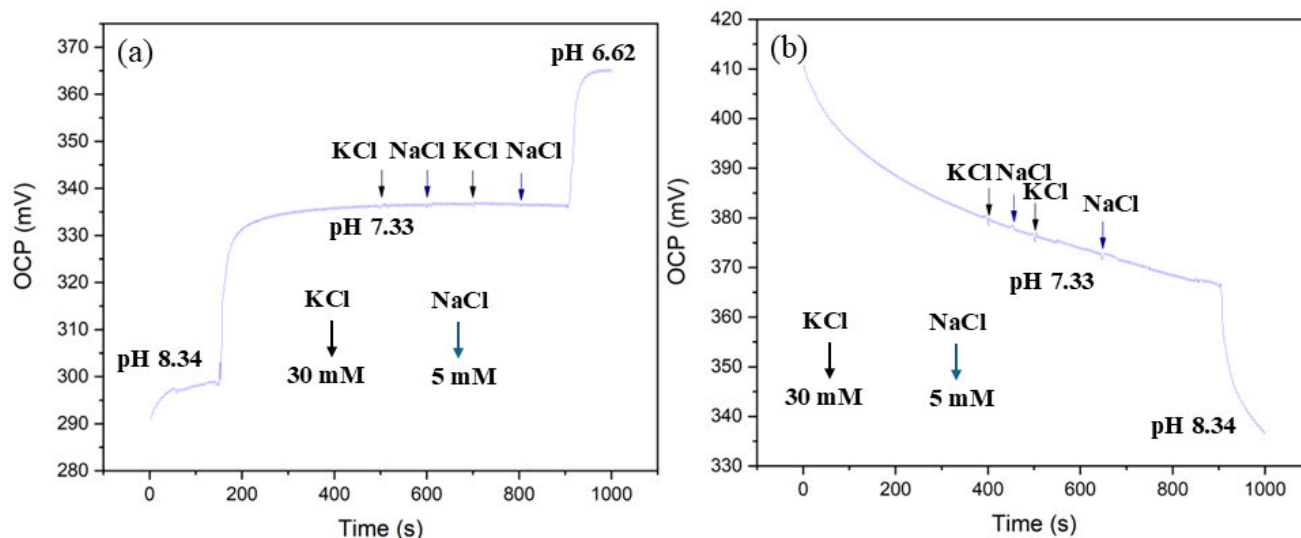


Fig. 10. Interference tests for ZnFe<sub>2</sub>O<sub>4</sub> pH sensor by adding 30 mM KCl and 5 mM NaCl in solution at neutral pH. The tests are performed by changing the pH from (a) basic to neutral pH and (b) neutral to basic pH.

our ZnFe<sub>2</sub>O<sub>4</sub> and ZnO -based sensors. ZnO-based sensor has shown higher hysteresis width compared to the other two types of sensors in this work. For the selection of the electrode type, it is crucial to consider eventual metal oxide dissolution effects. The dissolution depends on the metal solubility in the solution and the loading of the nanoparticle/microparticle on the surface [41]. ZnO can dissociate into Zn(II) and Zn(OH)<sup>+</sup> ions in aqueous solutions with alkaline or neutral pH conditions [40], [41], [42], [43]. On the other hand, there is no evidence of dissolution of ZnFe<sub>2</sub>O<sub>4</sub> reported so far in the literature. Thus, interference tests are performed with the ZnFe<sub>2</sub>O<sub>4</sub>-based sensor by using relevant interferent species, namely KCl and NaCl, at the physiological pH of 7.33 (close to the blood pH of 7.4). The measurement graph is shown in Fig. 10. During the measurement, 30 mM KCl is added followed by the successive addition of 5 mM NaCl. There is no significant effect on the potential response of the sensor proving an excellent pH sensing selectivity to interfering ions. In this work, we used the simple auto-combustion synthesis method to produce ZnO and ZnFe<sub>2</sub>O<sub>4</sub> particles based on our previous work [25], [26]. The electrochemical pH sensor response of the SPEs is improved by modification with the synthesized micromaterial/nanomaterial. The performance of the sensors can be further improved to have more control over the particle growth kinetics and the material structural properties. For instance, using appropriately selected surfactants during the synthesis can reduce particle aggregation. This would lead to an improvement in particle activity when incorporated on the electrode surface.

#### IV. CONCLUSION

In this work, ZnO and ZnFe<sub>2</sub>O<sub>4</sub> particles are successfully produced using a simple and cost-effective auto-combustion synthesis method. The materials are characterized by FESEM and XRD to understand their morphological and structural features. Commercial SPEs were modified with the developed particles and studied as new electrochemical sensors. First, the sensors are characterized using ferri/ferrocyanide redox

couple as a probe molecule *via* CV. Significant enhancement in the performance of bare carbon sensor is achieved in terms of sensitivity and rate constant using ZnO or ZnFe<sub>2</sub>O<sub>4</sub> particles. Successively, the electrodes' performance as pH sensor is studied by means of chronopotentiometric measurements. The hysteresis behavior of the sensors is improved by using the physiological pH loop (4.5–8.5–4.5). We observed that the stability of the pH sensors is affected by the addition of OH<sup>-</sup> ions in the test solution. Because of this, we propose the use of alternative stock solutions for pH change to obtain a stable steady-state signal upon the increase in the pH. Overall, the pH sensitivity of bare carbon sensor is increased (>55%) by using two different surface-modified sensors (ZnO or ZnFe<sub>2</sub>O<sub>4</sub>). Due to potential dissolution issues of the ZnO particles when in water-based solution and reduced hysteresis in pH sensing, interference studies are conducted at ZnFe<sub>2</sub>O<sub>4</sub>-modified electrodes and shown that the sensor is silent to potentially relevant interfering ions.

In this work, we choose to study ZnFe<sub>2</sub>O<sub>4</sub> due to its chemical stability, easy processing, low-cost synthesis, high surface area at nanoscale, easily tunable structure, and its n-type semiconducting and ferromagnetic nature with normal spinel structure. For continuous monitoring, no dissolution is expected due to its highly stable closely packed face-centered cubic structure which is crucial in pH sensing. Additionally, by incorporating surfactants in the synthesis process (hydrothermal or co-precipitation or sol-gel method), agglomeration can be avoided leveraging nanoscale properties which can lead to improved performance in the future work.

#### ACKNOWLEDGMENT

Mallikarjun Madagalam is with the Department of Physics and Astronomy (Semiconductor Physics), KU Leuven—University of Leuven, 3001 Leuven, Belgium, also with the Department of Applied Science and Technology, Politecnico di Torino, 10129 Turin, Italy, also with the Bio/CMOS Interfaces Laboratory, École Polytechnique Fédérale de Lausanne, 2000 Lausanne, Switzerland, and also with the National Interuniversity Consortium of Materials Science and Technology—Unit of Torino, Politecnico di Torino, 50121 Florence, Italy (e-mail: mallikarjun.madagalam@polito.it).

486 Filippo Franceschini is with the Department of Physics and Astronomy  
487 (Semiconductor Physics), KU Leuven—University of Leuven,  
488 3001 Leuven, Belgium.

489 Catarina Fernandes is with the Department of Electrical Engineer-  
490 ing (Micro and Nano Systems), KU Leuven—University of Leuven,  
491 3001 Leuven, Belgium.

492 Michele Rosito is with the Department of Applied Science and Tech-  
493 nology, Politecnico di Torino, 10129 Turin, Italy.

494 Elisa Padovano is with the Department of Applied Science and  
495 Technology, Politecnico di Torino, 10129 Turin, Italy, and also with  
496 the National Interuniversity Consortium of Materials Science and  
497 Technology—Unit of Torino, Politecnico di Torino, 50121 Florence, Italy.

498 Sandro Carrara is with the Bio/CMOS Interfaces Laboratory, École  
499 Polytechnique Fédérale de Lausanne, 2000 Lausanne, Switzerland.

500 Alberto Tagliaferro is with the Department of Applied Science  
501 and Technology, Politecnico di Torino, 10129 Turin, Italy, also with  
502 the National Interuniversity Consortium of Materials Science and  
503 Technology—Unit of Torino, Politecnico di Torino, 50121 Florence,  
504 Italy, and also with the Faculty of Science, Ontario Tech University  
505 (OntarioTechU), Oshawa, ON L1G 0C5, Canada.

506 Mattia Bartoli is with the National Interuniversity Consortium of  
507 Materials Science and Technology—Unit of Torino, Politecnico di Torino,  
508 50121 Florence, Italy, and also with the Center for Sustainable Future  
509 Technologies, Italian Institute of Technology, 10144 Turin, Italy.

510 Irene Taurino is with the Department of Physics and Astronomy  
511 (Semiconductor Physics) and the Department of Electrical Engineer-  
512 ing (Micro and Nano Systems), KU Leuven—University of Leuven,  
513 3001 Leuven, Belgium.

## REFERENCES

- 515 [1] M. T. Ghoneim et al., “Recent progress in electrochemical  
516 pH-sensing materials and configurations for biomedical applications,”  
517 *Chem. Rev.*, vol. 119, no. 8, pp. 5248–5297, Mar. 2019, doi:  
518 [10.1021/acs.chemrev.8b00655](https://doi.org/10.1021/acs.chemrev.8b00655).
- 519 [2] D. Wencel, T. Abel, and C. McDonagh, “Optical chemical pH  
520 sensors,” *Anal. Chem.*, vol. 86, no. 1, pp. 15–29, Jan. 2014, doi:  
521 [10.1021/ac4035168](https://doi.org/10.1021/ac4035168).
- 522 [3] Y. Qin, H.-J. Kwon, M. M. R. Howlader, and M. J. Deen, “Microfab-  
523 ricated electrochemical pH and free chlorine sensors for water quality  
524 monitoring: Recent advances and research challenges,” *RSC Adv.*, vol. 5,  
525 no. 85, pp. 69086–69109, 2015, doi: [10.1039/c5ra11291e](https://doi.org/10.1039/c5ra11291e).
- 526 [4] Y. Qin et al., “Integrated water quality monitoring system with pH, free  
527 chlorine, and temperature sensors,” *Sens. Actuators B, Chem.*, vol. 255,  
528 pp. 781–790, Feb. 2018, doi: [10.1016/j.snb.2017.07.188](https://doi.org/10.1016/j.snb.2017.07.188).
- 529 [5] M. Weston, S. Geng, and R. Chandrawati, “Food sensors: Challenges  
530 and opportunities,” *Adv. Mater. Technol.*, vol. 6, no. 5, May 2021,  
531 Art. no. 2001242, doi: [10.1002/admt.202001242](https://doi.org/10.1002/admt.202001242).
- 532 [6] L. Manjakkal, D. Szwagierczak, and R. Dahiya, “Metal oxides based  
533 electrochemical pH sensors: Current progress and future perspec-  
534 tives,” *Prog. Mater. Sci.*, vol. 109, Apr. 2020, Art. no. 100635, doi:  
535 [10.1016/j.pmatsci.2019.100635](https://doi.org/10.1016/j.pmatsci.2019.100635).
- 536 [7] M. Yuqing, C. Jianrong, and F. Keming, “New technology for the  
537 detection of pH,” *J. Biochem. Biophys. Methods*, vol. 63, no. 1, pp. 1–9,  
538 Apr. 2005, doi: [10.1016/j.jbbm.2005.02.001](https://doi.org/10.1016/j.jbbm.2005.02.001).
- 539 [8] P. Kurzweil, “Metal oxides and ion-exchanging surfaces as pH sensors  
540 in liquids: State-of-the-art and outlook,” *Sensors*, vol. 9, no. 6,  
541 pp. 4955–4985, Jun. 2009, doi: [10.3390/s90604955](https://doi.org/10.3390/s90604955).
- 542 [9] S. Zaman, M. H. Asif, A. Zainelabdin, G. Amin, O. Nur, and  
543 M. Willander, “CuO nanoflowers as an electrochemical pH sensor and  
544 the effect of pH on the growth,” *J. Electroanal. Chem.*, vol. 662, no. 2,  
545 pp. 421–425, Nov. 2011, doi: [10.1016/j.jelechem.2011.09.015](https://doi.org/10.1016/j.jelechem.2011.09.015).
- 546 [10] L. Manjakkal, K. Cvejic, J. Kulawik, K. Zaraska, D. Szwagierczak,  
547 and R. P. Socha, “Fabrication of thick film sensitive RuO<sub>2</sub>-TiO<sub>2</sub> and  
548 Ag/AgCl/KCl reference electrodes and their application for pH mea-  
549 surements,” *Sens. Actuators B, Chem.*, vol. 204, pp. 57–67, Dec. 2014,  
550 doi: [10.1016/j.snb.2014.07.067](https://doi.org/10.1016/j.snb.2014.07.067).
- 551 [11] J. Bai and B. Zhou, “Titanium dioxide nanomaterials for sensor applica-  
552 tions,” *Chem. Rev.*, vol. 114, no. 19, pp. 10131–10176, Oct. 2014, doi:  
553 [10.1021/cr400625j](https://doi.org/10.1021/cr400625j).
- 554 [12] A. Wei, L. Pan, and W. Huang, “Recent progress in the ZnO  
555 nanostructure-based sensors,” *Mater. Sci. Eng., B*, vol. 176, no. 18,  
556 pp. 1409–1421, Nov. 2011, doi: [10.1016/j.mseb.2011.09.005](https://doi.org/10.1016/j.mseb.2011.09.005).
- 557 [13] I. Yaroshenko et al., “Real-time water quality monitoring with chem-  
558 ical sensors,” *Sensors*, vol. 20, no. 12, p. 3432, Jun. 2020, doi:  
559 [10.3390/s20123432](https://doi.org/10.3390/s20123432).
- [14] S. Al-Hilli and M. Willander, “The pH response and sensing mech-  
anism of n-type ZnO/electrolyte interfaces,” *Sensors*, vol. 9, no. 9,  
pp. 7445–7480, Sep. 2009, doi: [10.3390/s90907445](https://doi.org/10.3390/s90907445).
- [15] J. Chou et al., “Characterization of flexible arrayed pH sensor based  
on nickel oxide films,” *IEEE Sensors J.*, vol. 18, no. 2, pp. 605–612,  
Jan. 2018, doi: [10.1109/JSEN.2017.2773143](https://doi.org/10.1109/JSEN.2017.2773143).
- [16] L. Manjakkal, B. Sakhivel, N. Gopalakrishnan, and R. Dahiya,  
“Printed flexible electrochemical pH sensors based on CuO nanorods,”  
*Sens. Actuators B, Chem.*, vol. 263, pp. 50–58, Jun. 2018, doi:  
[10.1016/j.snb.2018.02.092](https://doi.org/10.1016/j.snb.2018.02.092).
- [17] H.-J. Chung et al., “Stretchable, multiplexed pH sensors with  
demonstrations on rabbit and human hearts undergoing ischemia,”  
*Adv. Healthcare Mater.*, vol. 3, no. 1, pp. 59–68, Jan. 2014, doi:  
[10.1002/adhm.201300124](https://doi.org/10.1002/adhm.201300124).
- [18] L. Manjakkal, K. Cvejic, J. Kulawik, K. Zaraska, D. Szwagierczak, and  
G. Stojanovic, “Sensing mechanism of RuO<sub>2</sub>-SnO<sub>2</sub> thick film pH sen-  
sors studied by potentiometric method and electrochemical impedance  
spectroscopy,” *J. Electroanal. Chem.*, vol. 759, pp. 82–90, Dec. 2015,  
doi: [10.1016/j.jelechem.2015.10.036](https://doi.org/10.1016/j.jelechem.2015.10.036).
- [19] L. Manjakkal, E. Djurdjic, K. Cvejic, J. Kulawik, K. Zaraska, and  
D. Szwagierczak, “Electrochemical impedance spectroscopic analysis  
of RuO<sub>2</sub> based thick film pH sensors,” *Electrochimica Acta*, vol. 168,  
pp. 246–255, Jun. 2015, doi: [10.1016/j.electacta.2015.04.048](https://doi.org/10.1016/j.electacta.2015.04.048).
- [20] C.-W. Pan, J.-C. Chou, T.-P. Sun, and S.-K. Hsiung, “Development of  
the real-time pH sensing system for array sensors,” *Sens. Actua-  
tors B, Chem.*, vol. 108, nos. 1–2, pp. 870–876, Jul. 2005, doi:  
[10.1016/j.snb.2004.11.087](https://doi.org/10.1016/j.snb.2004.11.087).
- [21] L. Santos et al., “WO<sub>3</sub> nanoparticle-based conformable pH sensor,” *ACS  
Appl. Mater. Interface*, vol. 6, no. 15, pp. 12226–12234, Aug. 2014, doi:  
[10.1021/am501724h](https://doi.org/10.1021/am501724h).
- [22] C. Fernandes et al., “Unraveling the potential of a nanostructured  
Tungsten-Tungsten oxide thin film electrode as a bioresorbable mul-  
tichemical wound healing monitor,” *Adv. Mater. Technol.*, vol. 9, no. 10,  
May 2024, Art. no. 2302007, doi: [10.1002/admt.202302007](https://doi.org/10.1002/admt.202302007).
- [23] J. Kim et al., “Structural insights into multi-metal spinel oxide nanopar-  
ticles for boosting oxygen reduction electrocatalysis,” *Adv. Mater.*,  
vol. 34, no. 8, Feb. 2022, Art. no. 2107868, doi: [10.1002/adma.202107868](https://doi.org/10.1002/adma.202107868).
- [24] J. M. Gonçalves et al., “Sensing performances of spinel ferrites MFe<sub>2</sub>O<sub>4</sub>  
(M = Mg, Ni, Co, Mn, Cu and Zn) based electrochemical sensors: A  
review,” *Analytica Chim. Acta*, vol. 1233, Nov. 2022, Art. no. 340362,  
doi: [10.1016/j.aca.2022.340362](https://doi.org/10.1016/j.aca.2022.340362).
- [25] M. Madagalal et al., “Unraveling the effect of the chemical and  
structural composition of Zn<sub>x</sub>Ni<sub>1-x</sub>Fe<sub>2</sub>O<sub>4</sub> on the electron transfer at  
the electrochemical interface,” *Small Struct.*, vol. 4, no. 12, Dec. 2023,  
Art. no. 2300163, doi: [10.1002/ssstr.202300163](https://doi.org/10.1002/ssstr.202300163).
- [26] M. Madagalal et al., “Unveiling the effect of bi in ZnFe<sub>2</sub>O<sub>4</sub> nanopar-  
ticles in electrochemical sensors,” *Appl. Surf. Sci.*, vol. 673, Nov. 2024,  
Art. no. 160870, doi: [10.1016/j.apsusc.2024.160870](https://doi.org/10.1016/j.apsusc.2024.160870).
- [27] M. Madagalal et al., “Enhancing electrochemical sensor performance:  
Studies of electrodes tailored with ZnO/ZnFe<sub>2</sub>O<sub>4</sub> nanoparticles,” *Meat.  
Abstr.*, vol. 245, no. 47, p. 2627, Aug. 2024, doi: [10.1149/MA2024-01472627mtgabs](https://doi.org/10.1149/MA2024-01472627mtgabs).
- [28] M. Kumar, B. E. Kumara Swamy, C. Sravanthi, C. M. Praveen  
Kumar, and G. K. Jayaprakash, “NiFe<sub>2</sub>O<sub>4</sub> nanoparticle modified elec-  
trochemical sensor for the voltammetric study of folic acid and  
paracetamol,” *Mater. Chem. Phys.*, vol. 284, May 2022, Art. no. 126087,  
doi: [10.1016/j.matchemphys.2022.126087](https://doi.org/10.1016/j.matchemphys.2022.126087).
- [29] N. T. Anh et al., “An on-site and portable electrochemical sensing  
platform based on spinel zinc ferrite nanoparticles for the quality control  
of paracetamol in pharmaceutical samples,” *Nanosci. Adv.*, vol. 6, no. 1,  
pp. 256–267, 2024, doi: [10.1039/d3na00749a](https://doi.org/10.1039/d3na00749a).
- [30] M. Amiri, M. Salavati-Niasari, and A. Akbari, “Magnetic nanocarriers:  
Evolution of spinel ferrites for medical applications,” *Adv. Colloid  
Interface Sci.*, vol. 265, pp. 29–44, Mar. 2019, doi: [10.1016/j.cis.2019.01.003](https://doi.org/10.1016/j.cis.2019.01.003).
- [31] M. Madagalal, M. Bartoli, S. Carrara, and A. Tagliaferro,  
“ZnCr<sub>2-x</sub>Fe<sub>x</sub>O<sub>4</sub> nanoparticles-modified electrochemical sensors: A  
comparative study,” in *Proc. IEEE Sensors*, Oct. 2023, pp. 1–4, doi:  
[10.1109/sensors56945.2023.10325135](https://doi.org/10.1109/sensors56945.2023.10325135).
- [32] M. Madagalal, M. Bartoli, S. Carrara, and A. Tagliaferro,  
“ZnM<sub>x</sub>Fe<sub>2-x</sub>O<sub>4</sub> (M=Cr, Bi) nanoparticles-modified electrochemical sen-  
sors: Effect on sensitivity and first-order kinetic rate constant,” in  
*Proc. IEEE BioSensors Conf. (BioSensors)*, Jul. 2023, pp. 1–4, doi:  
[10.1109/biosensors58001.2023.10280910](https://doi.org/10.1109/biosensors58001.2023.10280910).

- 635 [33] A. C. F. M. Costa, E. Tortella, M. R. Morelli, M. Kaufman, and  
 636 R. H. G. A. Kiminami, "Effect of heating conditions during combustion  
 637 synthesis on the characteristics of  $\text{Ni}_{0.5}\text{Zn}_{0.5}\text{Fe}_2\text{O}_4$  nanopowders,"  
 638 *J. Mater. Sci.*, vol. 37, no. 17, pp. 3569–3572, Sep. 2002, doi:  
 639 [10.1023/a:1016528302082](https://doi.org/10.1023/a:1016528302082).
- 640 [34] A. J. Bard and L. R. Faulkner, *Electrochemical Methods Fundamentals  
 641 and Applications*. New York, NY, USA: Wiley, 2001.
- 642 [35] R. S. Nicholson, "Theory and application of cyclic voltammetry for  
 643 measurement of electrode reaction kinetics," *Anal. Chem.*, vol. 37,  
 644 no. 11, pp. 1351–1355, Oct. 1965.
- 645 [36] M. Madagalam, M. Bartoli, A. Tagliaferro, and S. Carrara, "Bismuth-  
 646 nanocomposites modified SPCEs for non-enzymatic electrochemical  
 647 sensors," *IEEE Sensors J.*, vol. 21, no. 9, pp. 11155–11162, May 2021,  
 648 doi: [10.1109/JSEN.2021.3059278](https://doi.org/10.1109/JSEN.2021.3059278).
- 649 [37] E. Laviron, "General expression of the linear potential sweep voltam-  
 650 mogram in the case of diffusionless electrochemical systems," *J.  
 651 Electroanal. Chem. Interfacial Electrochemistry*, vol. 101, no. 1,  
 652 pp. 19–28, Jul. 1979, doi: [10.1016/s0022-0728\(79\)80075-3](https://doi.org/10.1016/s0022-0728(79)80075-3).
- 653 [38] C.-N. Tsai, J. C. Chou, T. P. Sun, and S. K. Hsiung, "Study on  
 654 the time-dependent slow response of the tin oxide pH electrode,"  
 655 *IEEE Sensors J.*, vol. 6, no. 5, pp. 1243–1249, Oct. 2006, doi:  
 656 [10.1109/JSEN.2006.881364](https://doi.org/10.1109/JSEN.2006.881364).
- 657 [39] C. Fan et al., "Synthesis and electrocatalytic mechanism of ultra-  
 658 fine  $\text{MFe}_2\text{O}_4$  (M: Co, Ni, and Zn) nanocrystallites: M/Fe synergistic  
 659 effects on the electrochemical detection of Cu(II) and hydrogen evo-  
 660 lution reaction performances," *J. Mater. Chem. A*, vol. 9, no. 39,  
 661 pp. 22277–22290, 2021, doi: [10.1039/d1ta05646h](https://doi.org/10.1039/d1ta05646h).
- 662 [40] H. Zhang et al., "Use of metal oxide nanoparticle band gap to develop a  
 663 predictive paradigm for oxidative stress and acute pulmonary inflam-  
 664 mation," *ACS Nano*, vol. 6, no. 5, pp. 4349–4368, May 2012, doi:  
 665 [10.1021/nm3010087](https://doi.org/10.1021/nm3010087).
- 666 [41] M. Auffan, J. Rose, M. R. Wiesner, and J.-Y. Bottero, "Chemical stability  
 667 of metallic nanoparticles: A parameter controlling their potential cellular  
 668 toxicity in vitro," *Environ. Pollut.*, vol. 157, no. 4, pp. 1127–1133,  
 669 Apr. 2009, doi: [10.1016/j.envpol.2008.10.002](https://doi.org/10.1016/j.envpol.2008.10.002).
- 670 [42] T. Xia et al., "Decreased dissolution of ZnO by iron doping yields  
 671 nanoparticles with reduced toxicity in the rodent lung and zebrafish  
 672 embryos," *ACS Nano*, vol. 5, no. 2, pp. 1223–1235, Feb. 2011, doi:  
 673 [10.1021/nn1028482](https://doi.org/10.1021/nn1028482).
- 674 [43] T. Xia et al., "Comparison of the mechanism of toxicity of zinc oxide  
 675 and cerium oxide nanoparticles based on dissolution and oxidative stress  
 676 properties," *ACS Nano*, vol. 2, no. 10, pp. 2121–2134, Oct. 2008, doi:  
 677 [10.1021/nm800511k](https://doi.org/10.1021/nm800511k).



particular emphasis  
molecules.

**Filippo Franceschini** (Student Member, IEEE) received the B.Sc. degree in mechanical engineering from the Università degli Studi di Brescia, Brescia, Italy, and the M.Sc. (summa cum laude) degree in materials engineering from the Polytechnic University of Turin, Turin, Italy. He is currently pursuing the Ph.D. degree in physics with KU Leuven, Leuven, Belgium, as an FWO Fellow (Strategic Basic Research).

His research focuses on the intersection of materials science and electrocatalysis, with a particular emphasis on nonenzymatic electrooxidation of organic molecules.



materials and microfabrication techniques for implantable, bioresorbable electrochemical sensors.

**Catarina Fernandes** received the B.Sc. degree in micro- and nanotechnology engineering from the NOVA School of Science and Technology, NOVA University Lisbon, Portugal, in 2019, and the M.Sc. degree in nanoscience from Aarhus University, Aarhus, Denmark, in 2021. She is currently the Ph.D. degree with the Micro and Nano-Systems (MNS) Research Group, KU Leuven, Leuven, Belgium, under the supervision of Prof. Irene Taurino.

Her research focuses on developing novel materials and microfabrication techniques for implantable, bioresorbable electrochemical sensors.

**Michele Rosito** received the B.Sc. and M.Sc. degrees in materials engineering from Politecnico di Torino, Turin, Italy, in 2013 and 2020, respectively, where he is currently pursuing the Ph.D. degree in materials science and technology with the Department of Applied Science and Technology.

His current research interests include metal additive manufacturing, with a focus on laser powder bed fusion, aluminum alloys, and metal matrix composites, as well as materials characterization through XRD analysis.



**Mallikarjun Madagalam** (Student Member, IEEE) received the bachelor's degree in electronics and communication engineering from the Rajiv Gandhi University of Knowledge Technologies, Nuzvid, India, in 2014, the first master's degree in electronics from Halmstad University, Halmstad, Sweden, in 2017, and the second master's degree in nanotechnologies for ICTs from Politecnico di Torino, Turin, Italy, and from 2020, he pursued the Ph.D. degree on the effect of spinel nanomaterials on electron transfer at the electrochemical interfaces.

From November 2016 to February 2017, he was a Research Engineer with Halmstad University. While pursuing his second master's degree in Italy, he received full scholarship, international mobility grant from EDISU, and thesis abroad scholarship from Politecnico di Torino. From 2020 to 2021, he was a Research Assistant with the Sensing Technologies Laboratory of Prof. Paolo Lugli, Free University of Bolzano, Bolzano, Italy. During his Ph.D., he spent a period in the electrochemistry group of Prof. Irene Taurino at KU Leuven, Leuven, Belgium, and another period in the Bio/CMOS Interfaces Laboratory of Prof. Sandro Carrara at École Polytechnique Fédérale de Lausanne (EPFL), Lausanne, Switzerland.

Mr. Madagalam was awarded the Global Swede Award in 2016 by Swedish Ministry of Foreign Affairs and the Swedish Institute.

**Elisa Padovano** received the master's degree in environmental and cultural heritage chemistry from the University of Turin, Turin, Italy, in 2010, and the Ph.D. degree in materials science and technology from the Polytechnic University of Turin, Turin, in 2015.

In January 2011, she started her research fellowship at Polytechnic University of Turin. She is an Associate Professor at Politecnico di Torino, Turin. She is the author or co-author of more than 40 scientific articles published in international peer-review journals, and various presentations in international and national conferences in the field of materials science and engineering. Her research activity mainly focused on the investigation of the processing–structure–properties relationship of advanced materials fabricated by additive manufacturing techniques. She gained experience in the processing and characterization of innovative materials for different applications. The research activity is mainly focused on 1) the development of new polymer-based composites to be processed by selective laser sintering and fused filament fabrication techniques and 2) the processing of innovative metal materials by powder bed fusion technologies.



**Sandro Carrara** (Fellow, IEEE) received the Ph.D. degree in biochemistry and biophysics from the University of Padua, Padua, Italy, the master's degree in physics from the University of Genoa, Genoa, Italy, and the diploma degree in electronics from the National Institute of Technology, Albenga, Italy.

He was a former Professor with the University of Genoa and the University of Bologna, Bologna, Italy. From 2013 to 2014, he was appointed as a CASS Distinguished Lecturer and from 2017 to 2019, he was a IEEE Sensors Council Distinguished Lecturer. He is a Professor with the École Polytechnique Fédérale de Lausanne (EPFL), Lausanne, Switzerland, where he is the Head of the Bio/CMOS Interfaces Laboratory. His work has constantly received international recognition with several best-cited papers and best conference papers. Throughout his career, he published seven books with prestigious publishers such as Springer/NATURE and Cambridge University Press. He has more than 400 scientific publications and is the author of 19 patents/patent-requests.

Dr. Carrara is a member of the IEEE Sensors Council, where he was the Vice President of Publications. He also was a member of the Board of Governors (BoG) of the IEEE Circuits and Systems Society (CASS). He is the recipient of the IEEE Sensors Council Technical Achievement Award in 2016, and the Scientist Medal by the International Association of Advanced Materials in 2024. He has been the General Chairman of the premier worldwide international conference in the area of circuits and systems for biomedical applications, IEEE Biomedical Circuits and Systems (BioCAS), in 2014. He also has been the General Chairman of the 16th Edition of IEEE International Symposium on Medical Measurements and Applications (MeMeA), IEEE MeMeA, in 2021. He is a former Editor-in-Chief of the IEEE SENSORS Journal, one of the largest journals among 220 IEEE publications, and an Associate Editor of IEEE TRANSACTIONS ON BIOMEDICAL CIRCUITS AND SYSTEMS. He is also former Founding Editor-in-Chief of the Springer/NATURE journal titled *NanoBioScience*.



**Alberto Tagliaferro** received the M.Sc. degree in nuclear engineering and the Ph.D. degree in physics from the Polytechnic University of Turin, Turin, Italy.

He is an Associate Professor with the Applied Science and Technology Department, Polytechnic University of Turin. He is also the Head of the Carbon Group, a research group founded in 2002 focused on production, characterization, and the application of carbon-based materials. He has published more than 200 articles on

international peer-reviewed journals and has a five-year h-index of 35 as per google scholar.

Dr. Tagliaferro is a member of the Editorial Board of a number of journals. He is Chair of the Education Committee of the International Union for Vacuum Science, Technique, and Applications (IUVSTA).



**Mattia Bartoli** received the M.Sc. (summa cum laude) degree in organic chemistry from the University of Florence, Florence, Italy, in 2013, and a prize for the outstanding graduation project from Italian Chemical Society, and the Ph.D. degree in chemistry from the University of Florence, in 2017.

Dr. Bartoli joined the Biorefinery Research Group, University of Alberta, where he contributed to developing new materials for catalytic applications and new technologies. During this period, he also worked as the Head of Research and Development for ForgeHydrocarbon a spin-off company of University of Alberta solving several issues of the innovative lipid-to hydrocarbon technology for renewable hydrocarbon production. Thanks to his contribution, ForgeHydrocarbon was able to move from pilot to commercial stage. In 2018, he joined the Carbon Group, Polytechnic University of Turin, Turin, Italy, where he studied both production and use of carbon from thermochemical conversion of wastestreams for material science applications. Since 2021, he has been working on nanomaterials development at the Center for Sustainable Future Technologies—CSFT@POLITO. He recognizes the interdisciplinary nature of the carbon materials research sector and puts all his efforts into developing not merely one-case solutions but platforms that could originate solution trees useful for solving complex scenarios by integrating material science. He works in collaboration with the University of Miami leading the foundation of chemical formation route of the main families of carbon dots. Since 2019, he has been in collaboration with both École Polytechnique Fédérale de Lausanne (EPFL), Lausanne, Switzerland, and Politecnico di Torino, Turin, empirical proved Markus Tachiya theory highlighting the role of surface state on electron transfer rate. He is enlisted in the World's Top 2% Scientists list.

Dr. Bartoli is a Fellow of several scientific societies.

**Irene Taurino** (Member, IEEE) received the B.Sc. degree in biomedical engineering from Politecnico di Torino, Turin, Italy, the dual M.Sc. (summa cum laude) degree in biomedical engineering from Politecnico di Milano, Milan, Italy, and the Ph.D. degree in microsystems and microelectronics at École Polytechnique Fédérale de Lausanne (EPFL), Lausanne, Switzerland, in 2015, under the supervision of Prof. Giovanni De Micheli and Prof. Sandro Carrara, specializing in nanotechnology, microfabrication, electrochemistry, and microfluidics.

In 2014, she was a Visiting Student at Harvard-MIT Health Sciences and Technology, Cambridge, MA, USA, integrating an electrochemical device into a microfluidic cell culture system. She later conducted postdoctoral research at EPFL, contributing to teaching and supervision. From 2016 to 2021, she was with Industrial Research and Development, Aerosol Science and Technology, filing tens of patent applications (43 simple families). In June 2021, she became an Assistant Professor at KU Leuven, Leuven, Italy, jointly affiliated with the Electrical Engineering and Physics and Astronomy Departments. Her research focuses on advanced micro- and nanotechnologies for soft electrochemical platforms. Since May 2023, she has also been a collaborator (10%) at the Italian Institute of Technology (IIT).